Numerical and experimental study of product gas characteristics in premixed ammonia/methane/air laminar flames stabilised in a stagnation flow

Marina Kovaleva [a,b,*], Akihiro Hayakawa [a], Sophie Colson [a], Ekenechukwu C. Okafor [c], Taku Kudo [a], Agustin Valera-Medina [b], Hideaki Kobayashi [a]

[a] *Institute of Fluid Science, Tohoku University, 2-1-1 Katahira, Aoba-ku, Sendai, Miyagi 980-8577, Japan*
[b] *College of Physical Sciences and Engineering, Cardiff University, Queen's Buildings, Cardiff CF243AA, UK*
[c] *Fukushima Renewable Energy Institute, National Institute of Advanced Industrial Science and Technology (AIST), 2-2-9 Machiikedai, Koriyama, Fukushima 963-0298, Japan*

ARTICLE INFO

ABSTRACT

The adoption of ammonia/hydrocarbon fuel blends can be viewed as an intermediate step towards a hydrogen economy, hence the characterization of methane/ammonia flame product gas trends is essential for designing combustors for a broader range of low-carbon fuel blends while fulfilling strict NOx requirements. This paper describes the product gas content of laminar premixed ammonia/methane flames for a range of equivalence ratios and ammonia heat ratios ranging from 10% to 60%, using a strain stabilized burner at atmospheric pressure and room temperature. The optimal condition to reduce NOx emissions while maintaining below 100 ppm of unburnt NH_3 emissions was found to be at equivalence ratio of 1.20 for higher ammonia ratios, moving incrementally closer over 1.35 as the methane fuel content was increased. Meanwhile, the highest measured NO values were ~6,950 ppm at an equivalence ratio of 0.9, peaking at heat ratios of 30% to 40% at this equivalence ratio. Detailed reaction mechanisms were evaluated against the experimental data and rate constants of NO production/consumption steps featuring both NH and HNO intermediates and thermal NOx reactions were updated for Okafor's mechanism. Changes in reaction rate constants improved the mechanism accuracy for NO emissions in lean to stoichiometric flames. Meanwhile, in the rich region, modelled NO values were less responsive to changes in reaction constants, suggesting the need for an alternative approach to improve NO predictions for rich, high methane content flames. However, N_2O performance in the rich region could be improved, highlighting the significance of the $HNO+CO{\rightarrow}NH+CO_2$ reaction.

Introduction

Ammonia is an energy vector supported by a global demand to reduce CO_2 emissions as recent advancements in the research and application of this fuel [1,2,3] show its promise as a future green energy carrier. Therefore, 'ammonia as a fuel' has become a recent topic of interest to the extent of being included in policy decisions of some countries [4].

At time of writing, one of the most significant announcements came from the Japanese Ministry for Economy, Trade and Industry (METI) which released its Green Growth Strategy for achieving carbon neutrality by 2050 [5]. This strategy was also supported by the *Road Map for Fuel Ammonia*, which covered plans relating to Japan's ammonia fuel demand in power generation and marine sectors [6]. In the UK, the Department of Transport has recommended the launch of ammonia/-hydrogen marine vessels within the next 5–15 years, as detailed in the *Maritime 2050: Navigating the Future* paper [7]. To support these strategies, many manufacture facilities for green ammonia (ammonia produced through methods that are carbon-free and 100% renewable), have been announced such as initiatives in Australia, Denmark, Morocco, New Zealand [8,9]. This list also includes Saudi Arabia, of which NEOM and ACWA Power have pledged $5 billion towards the production of what is expected to become world's largest green ammonia/hydrogen

Nomenclature

A	pre-exponential factor in the Arrhenius equation (units: depend on reaction order)
E_a	activation constant in the Arrhenius equation (cal/mol)
E_{NH_3}	ammonia heat ratio
k	reaction rate constant (unit, assuming second order reaction: $cm^3/s \cdot mol$
LHV	lower heating value (unit: kJ/mol)
LHV_{CH4}	lower heating value of methane (unit: kJ/mol)
LHV_{NH3}	lower heating value of ammonia (unit: kJ/mol)
n	temperature exponent in the Arrhenius equation
$(p_0, \ T_0)$	evaluated at standard temperature and pressure
Q_d	dilution gas flowrate (unit: m³/s)
$Q_{d,N}$	dilution gas flowrate during the Nth sampling (unit: m³/s)
Q_s	relative sample gas flowrate (unit: m³/s)
$Q_{s,1}$	relative sample gas flowrate (unit: m³/s), taken during the 1st sampling
$Q_{s,2}$	relative sample gas flowrate (unit: m³/s), taken during the 2nd sampling
Re	Reynolds number
T	temperature (unit: K)
X_i	mole fraction of object gas I (unit: mol)
$X_{i,1}$	mole fraction of object gas i, measured in the product gas during the 1st sampling (unit: mol)
$X_{i,2}$	mole fraction of object gas i, measured in the product gas during the 2nd sampling (unit: mol)
x_i	mole fraction of species, i
X_I	derived partial term for the uncertainty of arbitrary value I with respect to X_i
Z	dilution ratio in sampled gas
Z_1	dilution ratio in sampled gas, calculated for the 1st sampling
Z_2	dilution ratio in sampled gas, calculated for the 2nd sampling
δI	the uncertainty of arbitrary value, I
$\Xi_{tr,1}$	mole fraction of the tracer species in the dilution gas of the 1st sampling (unit: mol)
$\Xi_{tr,2}$	mole fraction of the tracer species in the dilution gas of the 2nd sampling (unit: mol)
$\xi_{tr,1}$	mole fraction of the tracer species measured during the 1st sampling (unit: mol)
$\xi_{tr,2}$	mole fraction of the tracer species measured during the 2nd sampling (unit: mol)
φ	equivalence ratio
$\omega_{s,k}$	magnitude pf the rate of species production (units: mol/m2s)

plant [10].

Compared to storage and transportation through liquid hydrogen or compressed gaseous hydrogen, ammonia is a safer solution with already established infrastructure. Despite costs associated with the initial conversion from hydrogen to ammonia, ammonia is estimated to be 26 to 30 times cheaper for long term storage per kilogram of hydrogen [11] due to its high boiling point of -33.3 °C, relative to hydrogen. Rather than undergoing the expense of converting ammonia back to hydrogen, there is a significant benefit in utilising ammonia directly as a fuel. Some studies have already explored pure ammonia combustion characteristics finding that high fuel-NO production [12], low laminar burning velocity [15], high ignition energy and a narrow stability range [13,14] to be challenges to its direct use. Doping with a more reactive fuel such as methane or hydrogen is often suggested as a method towards improving these characteristics. Hence, to aid the transition from a carbon-based to a hydrogen-based energy economy, a study of the product gas emissions of methane/ammonia fuel mixtures are relevant to developing combustor designs that meet future global warming regulatory targets.

Some studies [16,17] have noted that in ammonia/methane oxidation, NOx production is strongly correlated to the shared dependence of NO pathways on the H, O and OH radical pool, rather than through direct interaction of ammonia and methane oxidation pathways. Though most hydrocarbon-optimised mechanisms contain nitrogen chemistry, additional nitrogen species reactions are often neglected. For example, the GRI 3.0 mechanism excludes all reactions involving N_2H_2 and N_2H_3 species which have high sensitivity to ammonia flame laminar burning velocity as well as their reactions to produce NNH, the consumption of which has high NO sensitivity [17]. A review of nitrogen chemistry in combustion by Glarborg et al. [18] also explains how the addition of hydrocarbons in ammonia combustion opens additional NO pathways, (for example through the reaction of methyl and amine radicals), and that these interactions may limit the accuracy of modelling predictions, especially under rich conditions.

Turbulent flame emissions of ammonia/methane flames, especially in swirl burner configurations have been widely studied. However, uncertainty introduced from complex turbulence-chemistry interactions have led to laminar flame configurations being preferable for the validation of reaction kinetics. Therefore, the present study employs a laminar, stagnation-stabilised burner configuration [53] and its counterpart 1D numerical model for modelling reaction chemistry. The stabilised flame burner configuration enhances the stability range of high ammonia content blends, creating a local flow stagnation. Furthermore, the heated top plate present in this configuration allows a wall temperature as a boundary condition input for the numerical model, allowing for a direct chemistry comparison with the one-dimensional, laminar, premixed, burner-stabilised flame model.

Laminar ammonia/methane flames have previously been experimentally studied in relation to NO and CO emissions by Ramos et al. [25] and Rocha et al. [26], suggesting the best correlations with numerical models occurring at an equivalence ratio of 1.0 compared to 0.9 and 0.95 Other laminar ammonia/methane flame studies by Konnov et al. [27] and Henshaw et al. [28] agree that peak NOx emissions occur near stoichiometry, though the ammonia content of the flames studied is very low. More recently, the work of Brackmann et al. [29] showed methane flames doped with 5200 ppm of NH_3 to be stabilised through a stagnation plane and modelled with the equivalent CHEMKIN module for kinetic chemistry evaluation. While the mechanism developed by Glarborg and Mendiara [30] was in good agreement for predicting NO emissions of the flame, it was not able to capture the downstream positional shift for the ammonia-doped flames, highlighting the importance of validating detailed combustion mechanisms through both chemistry profiles and other flame parameters [29]. Finally, validation of lean NH_3/ CH_4 flames has also previously been conducted by Colson et al. [47], through a combined evaluation of NO and OH profiles and extinction stretch rate in counterflow flames. This study identified the mechanisms of UCSD (University of California, San Diego) and Okafor et al. as having the best performance, prompting their further analysis in the present work.

Therefore, this study evaluates for the first-time, laminar ammonia/methane product gas characteristics across the full range of equivalence ratios for which the flame was stable, and ammonia heat ratios ranging from 10% to 60% at atmospheric pressure using the dual gas dilution method. The objective of this study is to find the optimal operating conditions for low NO and NH_3 production, also considering other harmful species HCN, N_2O and NO_2, rarely investigated in ammonia/methane flame demonstrations until now. The resulting exhaust gas
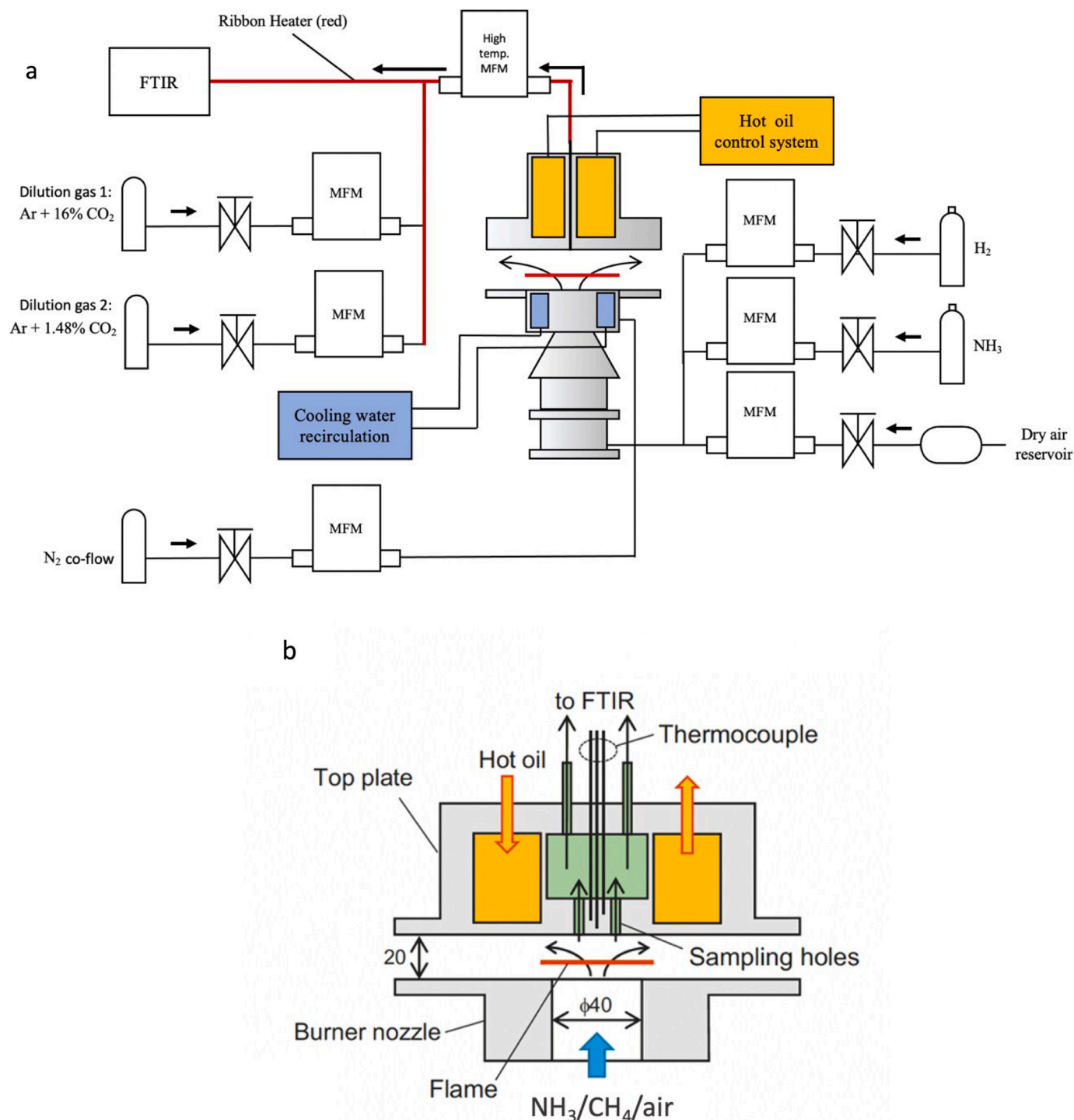
Fig. 1. Schematic diagram of the experiment: gas supply and sampling lines (a), schematic and dimensions of stagnation burner (b).
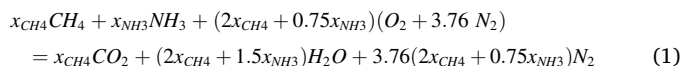
values provide validation data for one-dimensional numerical modelling to aid the understanding of chemical kinetics and reaction constant tuning in detailed ammonia/methane reaction mechanisms.

Experimental apparatus and procedures

Emissions of ammonia/methane flames were measured experimentally using a fully premixed laminar stagnation burner setup validated in previous work [31] and described in Fig. 1a. A nozzle burner with an outlet diameter of 40 mm was used in this study, shown in Fig. 1b and 1c. The gas components (dry air, ammonia, and methane) were mixed

before being injected into the bottom of the burner. The flat premixed burner flame was stabilised by a stagnation top plate circulating temperature-controlled oil to maintain a constant wall temperature, while water was injected into the bottom plate for cooling. For stabilisation, the burner was placed in the quartz tube and an outer co-flow of nitrogen gas was used as a curtain to shield around the flame edge.

The blends studied were defined by first considering Eq. (1) as the reaction for ideal ammonia/methane oxidation at stoichiometry:
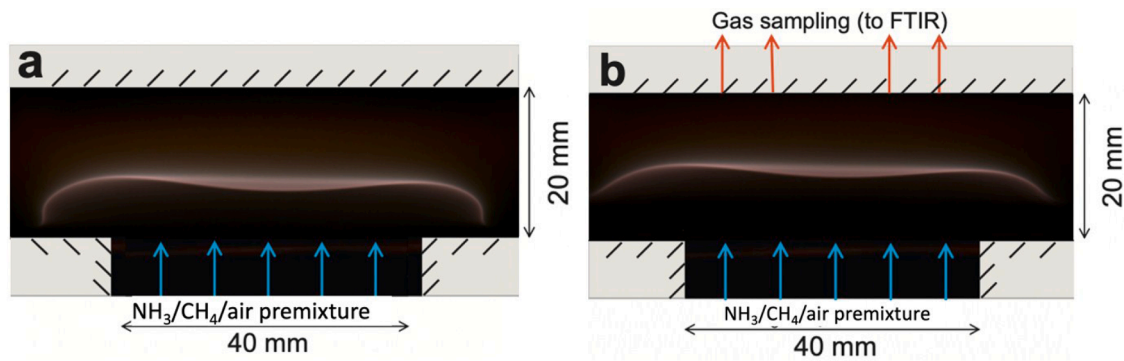
$$x_{CH4}CH_4 + x_{NH3}NH_3 + (2x_{CH4} + 0.75x_{NH3})(O_2 + 3.76\ N_2)$$
$$= x_{CH4}CO_2 + (2x_{CH4} + 1.5x_{NH3})H_2O + 3.76(2x_{CH4} + 0.75x_{NH3})N_2 \quad (1)$$

Fig. 2. Images of strain stabilised flame at E_{NH3}=20% and φ=1, without sampling and nitrogen curtain (a) and with sampling and nitrogen curtain (b).

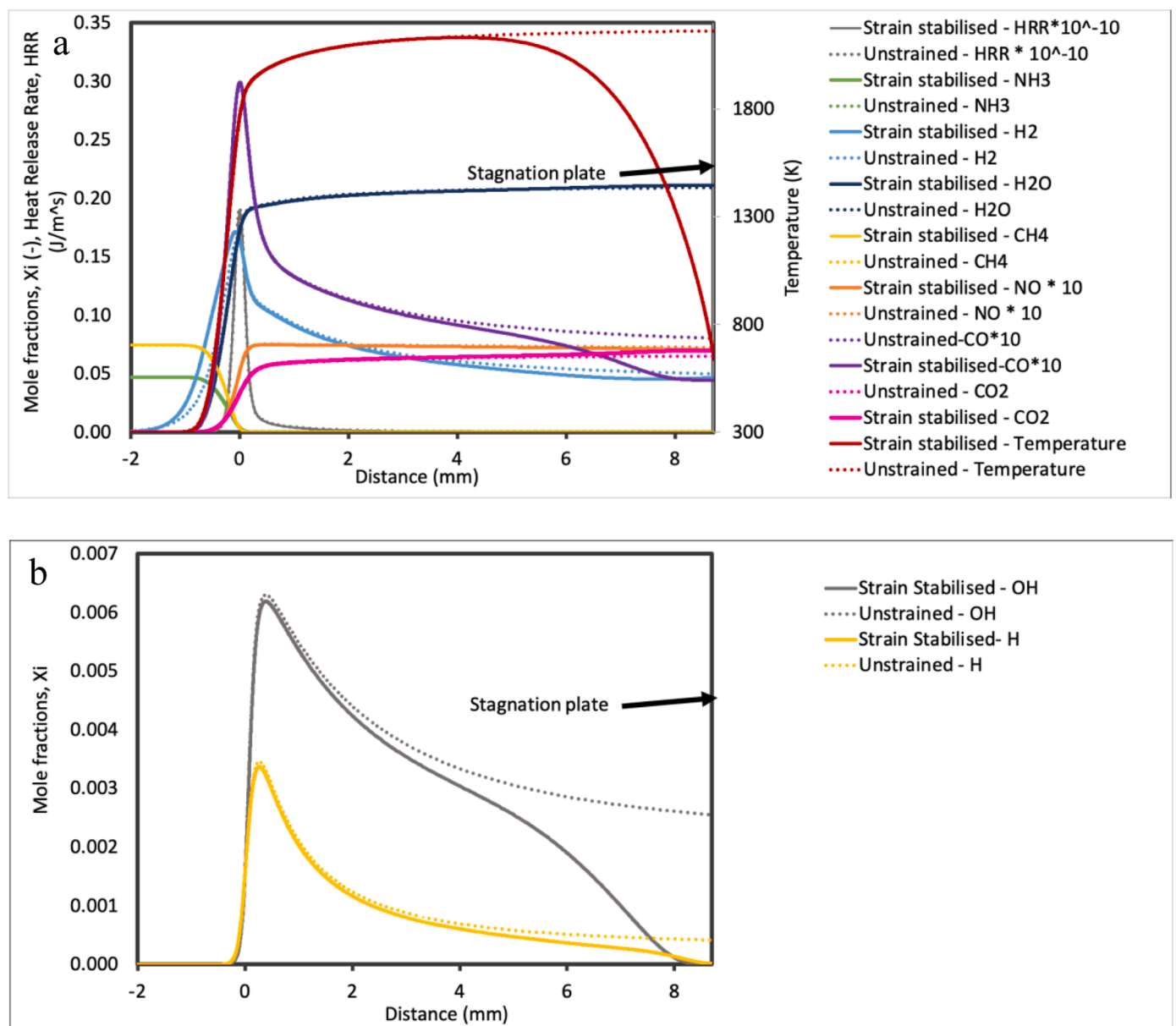**Fig. 3.** Flame profile of laminar premixed strained and unstrained numerical models along combustor length for a flame composition E_{NH3}=20% and φ=1.0, using Okafor's mechanism, for a) all product gases and b) OH and H [17].
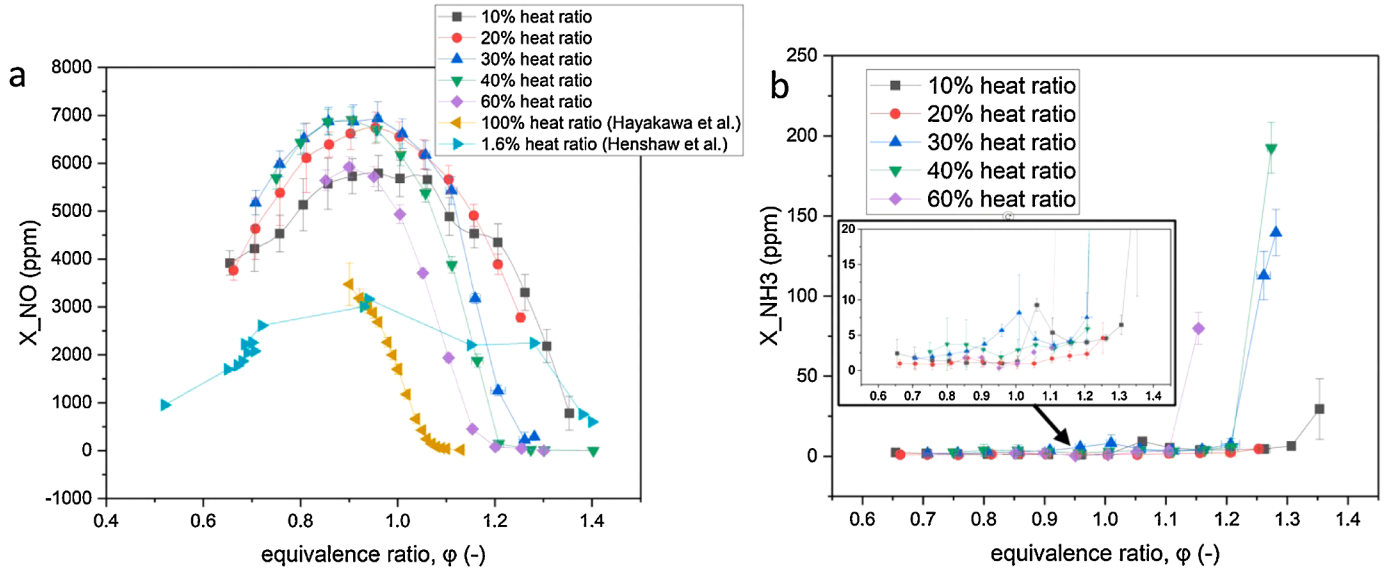
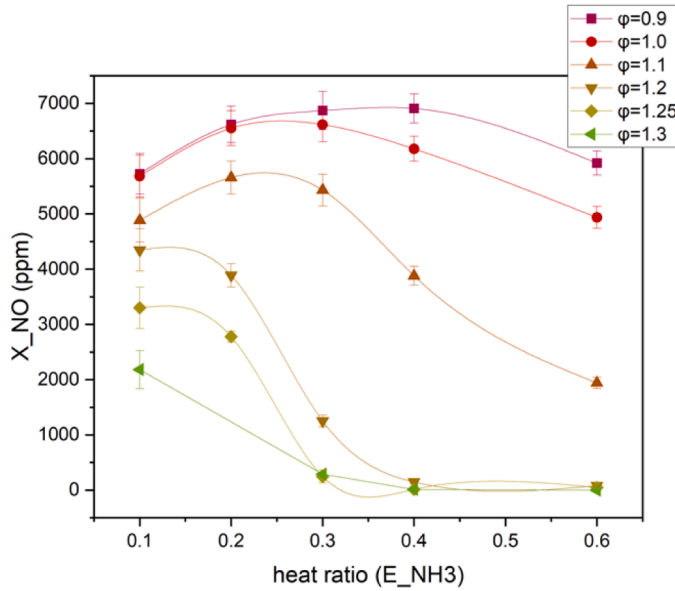**Fig. 4.** Measured product gas emissions by equivalence ratio for NO (a) and NH_3 (b).

Fig. 5. Measured product gas emissions by heat ratio for NO.

where x_{CH_4}, x_{NH_3} and x_{O_2} are the mole fractions of CH_4, NH_3, and O_2 respectively. The ratio of ammonia to methane in the fuel blend was defined by ammonia heat ratio, E_{NH_3}, as be expressed by Eq. 2:

$$E_{NH_3} = \frac{x_{NH_3} LHV_{NH_3}}{x_{NH_3} LHV_{NH_3} + x_{CH_4} LHV_{CH_4}} \times 100\% \qquad (2)$$

Where *LHV* is the lower heating value of the fuels ($LHV_{CH_4} = 802.30$ kJ/mol, $LHV_{NH_3} = 316.84$ kJ/mol). The air content was defined in terms of equivalence ratio, ϕ, given in Equation 3:

$$\phi = \frac{fuel-to-oxidizer\ ratio}{(fuel-to-oxidiser\ ratio)_{stoichiometry}} = \frac{\frac{x_{CH_4}+x_{NH_3}}{x_{O_2}}}{\left(\frac{x_{CH_4}+x_{NH_3}}{x_{O_2}}\right)_{stoich}} \qquad (3)$$

In the present study, the ammonia heat ratio, E_{NH_3} was varied between 10% to 60%, for the full range of equivalence ratios, φ, (defined by Eq. (3)) for which the flame was stable. The flowrate of the ammonia,

methane and dry air was controlled through a mass flow metre, needle valve and pressure regulator combination. The mass flowmeters were of KOFLOC3760 series with ±1.0% full scale accuracy and marked as MFM in Fig. 1.

The dual dilution gas sampling method was used to calculate species outside the measured range of the Fourier transform infrared gas analyser (Best Instruments, BOB2000FT) [32]. The dilution gas mixtures (consisting of carbon dioxide as the tracer species and argon gas as the base) were injected downstream of the sampling probe to dilute the product gas entering the analyser, allowing for measurement outside of the gas analyser range. Utilising two dilution gases is required when the dilution gas tracer species is also present at an unknown concentration in the combustion product gas, such as is the case for carbon dioxide in hydrocarbon-based flames. Furthermore, a simpler calculation by comparing the change in the sampling gas flowrate, Q_s is often not possible as Q_s is difficult to measure quantitatively. This is due to the conversion factor required for the calibration of a mass flow metre, which can only be determined for a known gas composition maintained at constant temperature and pressure. However, sampling the product gas twice at each condition, using two different dilution gas tracer species (carbon dioxide) concentrations, enables solving the product gas equations as simultaneous equations, reducing the number of unknown variables.

All equations for the dual dilution gas sampling method have been derived by Hayakawa et al. [32]. This includes Eq. (4) and Eq. (5) for calculating the dilution ratio, Z and hence the true value of the object gas through the analyser, X_i. In this case, the object gas values for the first and second sampling must be equal, $X_{i,1} = X_{i,2} = X_i$ and the relative sampling gas flowrate of $Q_s = Q_{s,1} = Q_{s,2}$ must be kept constant for each measurement, as confirmed by the high temperature mass flow metre (Hitachi Metals Ltd, SFC1480FX Series), shown in the experimental diagram given by Fig. 1. Eq. (4) shows that the mole fraction of species i, in object gas X_i can be expressed in terms of mole fractions of dilution gas tracer species 1 and 2 (corresponding to $\Xi_{tr,1} = 16\%$ and $\Xi_{tr,2} = 1.48\%$ in the present study) and the measured mole fraction of the tracer species in the measured product gas samples ($\xi_{tr,1}$ and $\xi_{tr,2}$).

$$X_{i,1} = Z_1 x_{i,1}$$
$$= \left\{ 1 + \frac{(\xi_{tr,1} - \xi_{tr,2}) Q_{d,1}(p_0,\ T_0)}{(\Xi_{tr,1} - \xi_{tr,1}) Q_{d,1}(p_0,\ T_0) - (\Xi_{tr,2} - \xi_{tr,2}) Q_{d,2}(p_0,\ T_0)} \right\} \cdot x_{i,1} \qquad (4)$$

Fig. 6. Measured product gas emissions by equivalence ratio for NO_2 (a), N_2O (b), CO (c), HCN (d).

$$X_{i,2} = Z_2 x_{i,2}$$
$$= \left\{ 1 + \frac{(\xi_{tr,1} - \xi_{tr,2}) Q_{d,1}(p_0,\ T_0)}{(\Xi_{tr,1} - \xi_{tr,1}) Q_{d,1}(p_0,\ T_0) - (\Xi_{tr,2} - \xi_{tr,2}) Q_{d,2}(p_0,\ T_0)} \right\} \cdot x_{i,2} \quad (5)$$
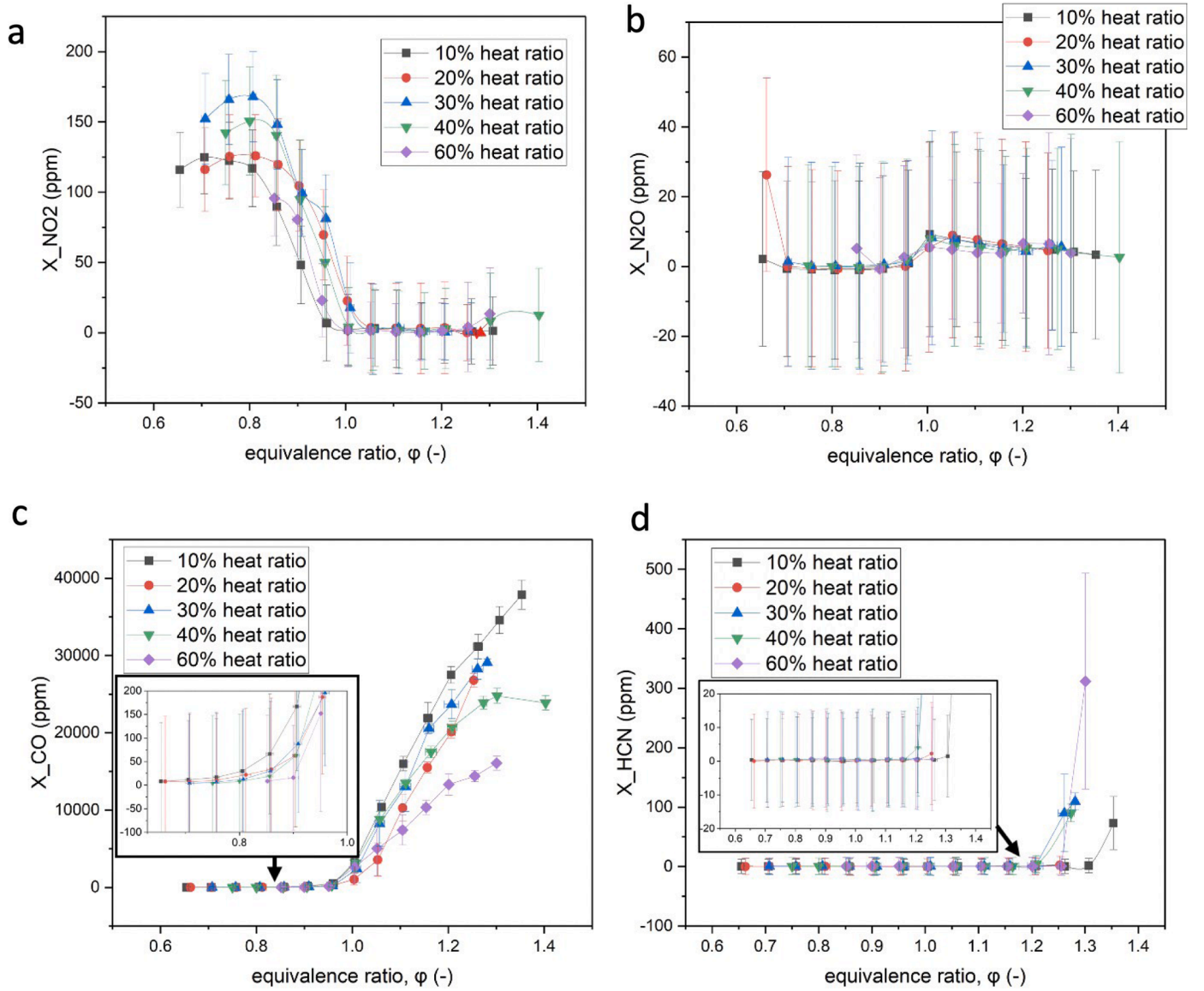
sampling ($\delta Q_{d,1}$, $\delta Q_{d,2}$) and finally, $\delta x_{i,1}$ as the uncertainty of the measured species in the first sampling by the gas analyser. X_{Ξ_1}, X_{Ξ_2}, X_{ξ_1}, X_{ξ_2}, X_{Q_1}, X_{Q_2}, X_x, represent the partial derivative of each source of uncertainty with respect to $X_{i,1}$, the object gas value.

$$\delta X_{i,1} = \sqrt{\left(X_{\Xi_1} \delta \Xi_{tr,1}\right)^2 + \left(X_{\Xi_2} \delta \Xi_{tr,2}\right)^2 + \left(X_{\xi_1} \delta \xi_{tr,1}\right)^2 + \left(X_{\xi_2} \delta \xi_{tr,2}\right)^2 + \left(X_{Q_1} \delta Q_{d,1}\right)^2 + \left(X_{Q_2} \delta Q_{d,2}\right)^2 + \left(X_x \delta x_{i,1}\right)^2} \qquad (6)$$

Hayakawa et al. [32] also quantifies the uncertainty of measuring product gas emissions with the dual dilution gas sampling method. The uncertainty used in the present work was given as the summation of uncertainty through repeat measurements and combined with the uncertainty of the dilution gas method, expressed by Eq. (6) for the first product gas sampling. This is expressed in terms of uncertainty of the tracer species in the first and second dilution gases ($\delta \Xi_{tr,1}$, $\delta \Xi_{tr,2}$), the uncertainty of measuring the tracer species in the product gas during the first and second sampling ($\delta \xi_{tr,1}$, $\delta \xi_{tr,2}$), the uncertainty in measuring the volumetric flowrate of the dilution gas during the first and second

The equivalence ratio uncertainty is derived from the uncertainty of mass flow meters and fluctuation in flow across the full sampling period, taken by a datalogger (Hioki MEMORY HiLOGGER LR8450), demonstrated by uncertainty bars in Section 3 of this work. Equally, the uncertainty of the heat ratio was calculated through measuring the fluctuation of methane and ammonia mass flowrate and this was deemed negligible as all values were calculated to be within ±0.05% of the full heat ratio percentage. Since all experimental and numerical
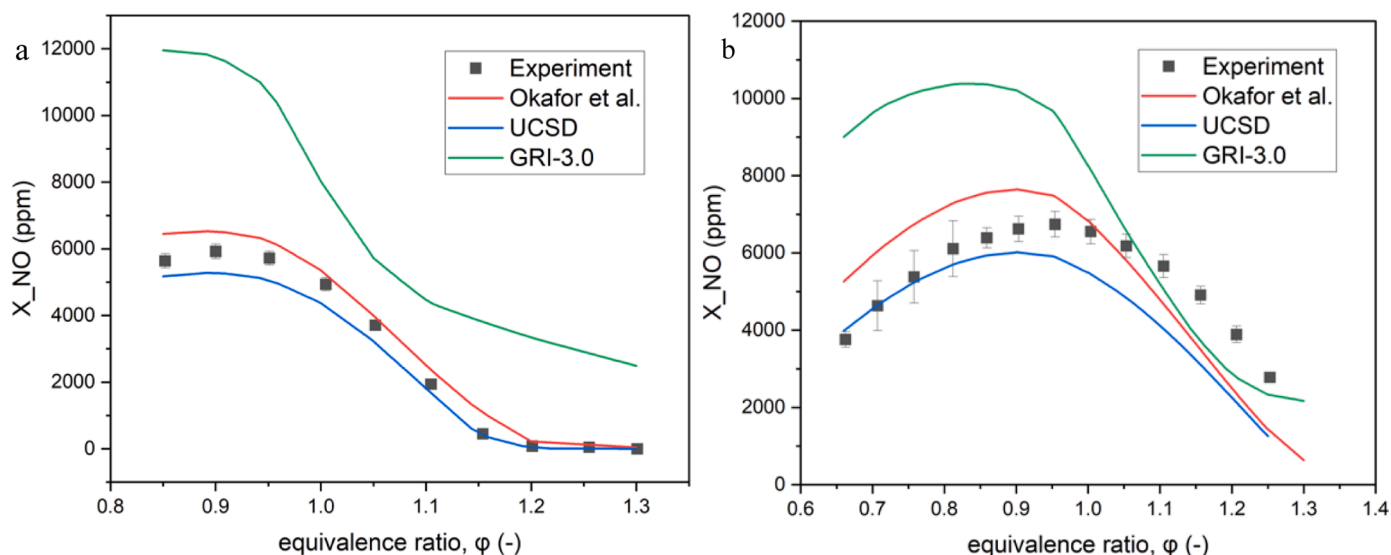
Fig. 7. A comparison of experimental NO results with numerical simulation results, for E_{NH3} = 20% (a) and 60% (b) conditions.
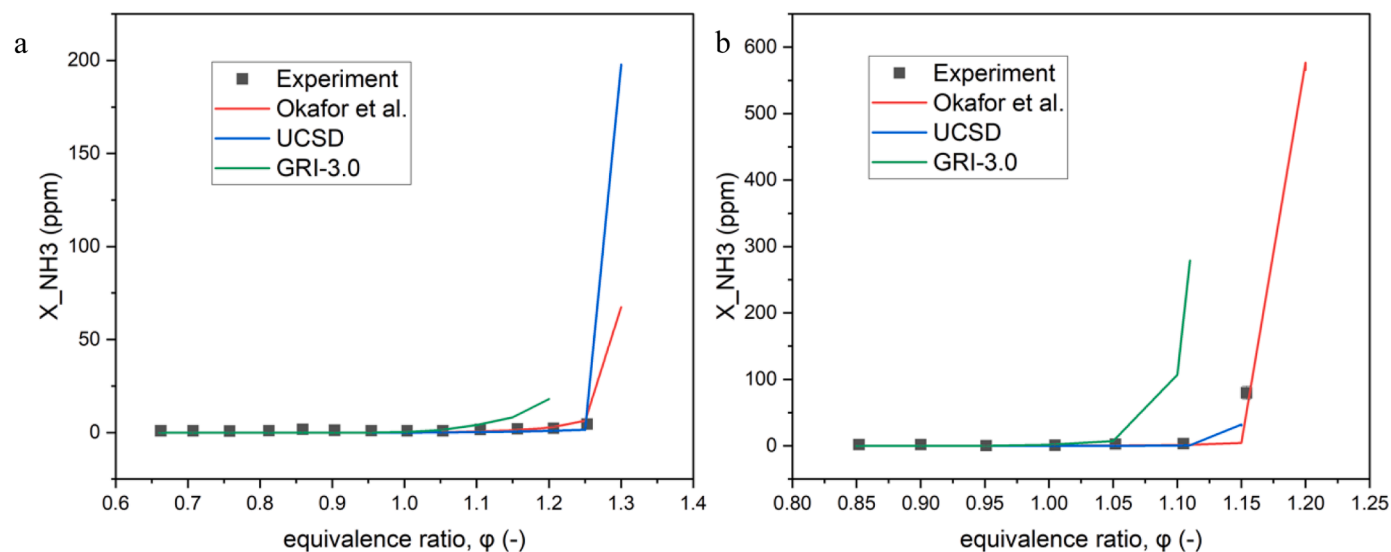

Fig. 8. A comparison of experimental NH_3 results with numerical simulation results, for E_{NH3} = 20% (a) and 60% (b) conditions.

values were measured as a percentage of total gas content (including water), for the purpose of fundamental analysis they will be reported as such.

The dilution gas and product gas lines were heated to above 393 K to ensure that no water condensation occurred in the piping. Thermocouples were used to monitor the temperature of the heated pipes (marked in red in Fig. 1) at regular intervals along the heated section. The gases were sampled through 18 holes 4.2 mm in diameter drilled through the centre of the stagnation plate [31]. The stagnation plate also contained three thermocouples at staggered depths used to estimate the wall temperature necessary as a boundary condition for numerical modelling. The sampling flowrate was kept as low as possible, such as to limit the interference on the flame. Fig. 2 provides images showing the effect of sampling and 5SLM flowrate nitrogen curtain on the flame profile. The effects of the nitrogen curtain flowrate, stagnation plate temperature and sampling rate are deemed negligible compared to other experimental uncertainties through results and further discussion given in the supplementary materials.

Numerical modelling was conducted through the CHEMKIN-Pro 2021 R1 [33] premixed laminar burner-stabilised stagnation flame model. Flame profile characteristics of the strained and unstrained numerical models are shown in Fig. 3, with the position of both flames aligned such that the distance along the combustor length at which peak heat release occurs is at 0 mm. For the strained flame, the temperature of 637 K at the stagnation plane was taken from measured thermocouple data for the plotted flame mixture (E_{NH3}=20% and φ=1.0). Hence, a key difference in the configuration is the temperature profile at the outlet. As the temperature between the strained and unstrained flame trends diverges (at approximately 4 mm), the CO trends also diverge significantly, with proportionally smaller changes for H_2, NO, CO_2. In strain-stabilised flames, CO_2 production is higher and CO production is lower at the outlet. This difference can be described through the primary conversion route between CO and CO_2, given by $CO + OH \rightarrow CO_2 + H$ [46]. The trend for CO follows closely the trend for OH, showing rapid consumption of OH to CO_2 near the stagnation plate.

Despite ammonia having a higher ignition energy, Fig. 3. shows that ammonia and methane are consumed at around the same distance along the combustor length. H_2 is produced early in the flame and then consumed in the post flame zone. NO trends stabilise, decreasing only slightly after the peak heat release zone and subsequent reactions of H_2
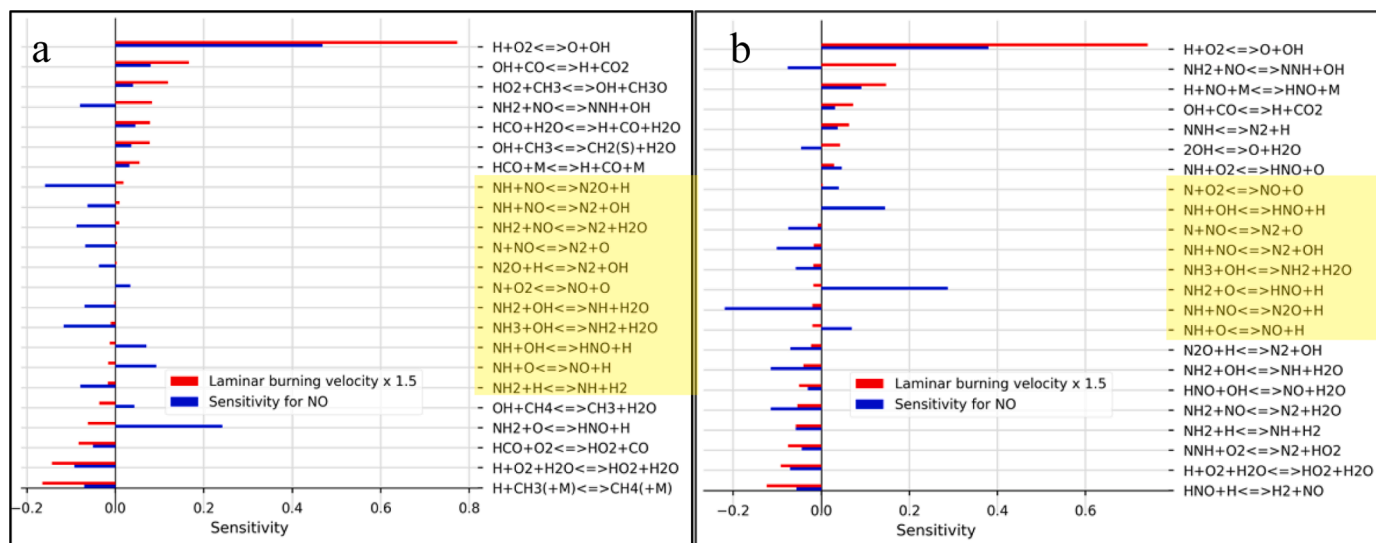
Fig. 9. Reactions with highest NO sensitivity and ordered by their corresponding laminar burning velocity sensitivity for $E_{NH3} = 20\%$ (a) and 60% (b) at φ=0.85, using the mechanism of Okafor et al.

and CO species in the post-flame zone have minimal impact relative to the reactions in the reaction zone. However, simultaneously to the decrease in H and H_2 concentrations, H_2O continues to increase in concentration in the post flame zone. Most of the NO is formed initially in the reaction zone and despite the high temperatures of the post-flame zone, NO does not continue to significantly change after this point. There is only a small influence of the stagnation plate on the NO concentration, and since all the NH_3 has been consumed, there is no further consumption of NO through NH_3 beyond this point. However, studies of Otomo et al. [49] have shown that for ammonia/air flames, this gradient is highly dependant on equivalence ratio, and at rich conditions, NO in the post-flame zone can be reduced through unburnt NH_3.

For the numerical modelling, the following three mechanisms were selected:

- The University of California, San Diego (UCSD) mechanism [34], using the 2016 version of the full mechanism and including the nitrogen-hydrocarbon subset from the 2018 update, with the combined mechanism using 68 species and 311 reactions.
- Okafor's mechanism [17] using 59 species and 356 reactions and is based on GRI Mech 3.0, with additional reactions and species from Tian's mechanism for NH_3/CH_4 mixtures. It has been optimised on the laminar burning velocity of CH_4/NH_3 mixtures of $E_{NH3} = 10\%$, 20%, 30% at 0.1 MPa and validated in subsequent studies, for example for laminar burning velocity of NH_3/CH_4 flames at higher pressures [19], emissions of ammonia/air flames [31] and for laminar burning velocity of NH_3/H_2 flames [20]
- GRI Mech 3.0 [35] is contains of 53 species and 325 reactions. GRI Mech 3.0 is one of the most popular mechanisms for modelling hydrocarbon fuels, though it does contain some nitrogen chemistry, including NH_3 species reactions.

Due to the variation of laminar burning across the range of studied equivalence ratios, the inlet velocity of the premixture was variable. This allowed range of equivalence ratios studied to be extended further into the lean and rich regions without encountering flashback and blow-off. The inlet velocity was calculated through curve fitting, based on Okafor's reaction model [17], which has been specifically optimized for laminar burning velocity of ammonia/methane mixtures. The laminar burning velocity curve for each fuel mixture was multiplied by a constant value, c to calculate the resulting mixture inlet velocity. The multiplier constant c values were selected to maintain a stable flame at

all conditions and above the laminar burning velocity value but within the laminar flow region. The Reynold's number at each condition was calculated to ensure that the flame was in the laminar region (Re<2300), with values provided in the supplementary data. A validation study (also detailed in the supplementary materials) was conducted to confirm that any impact of adjusting c were negligible compared to the uncertainty of the experiment calculated through the dilution gas method. Furthermore, as mixture inlet velocity is a required parameter in the numerical simulation, any variation in emissions occurring from inlet velocity is accounted for by the numerical model.

Results and discussion

Experimental results

Fig. 4 shows the variation in of NO and NH_3 with ammonia heat ratio (E_{NH3}) and equivalence ratio, φ. The NO trend was reported alongside data from other sources which extended the trend to the most extreme ammonia heat ratio conditions. The data for the 100% ammonia blend was taken from Hayakawa et al. [31] using the same configuration as the current study, while data from Henshaw et al. [28] was taken for the ammonia volume fraction of 4% ($\sim E_{NH3} = 1.6\%$) under a perforated flat flame burner configuration.

Fig. 4 shows peak NO emissions occurring at near stoichiometry, while the window of unburnt ammonia and low NO emissions simultaneously moves further towards the rich region as methane fuel content was increased. Therefore, the optimal conditions for which low NO_x and NH_3 emissions occurred was at $\varphi =\sim 1.35$ to 1.20 corresponding to fuel blends of $E_{NH3} = 10\%$ to 60% of premixed ammonia/methane fuel mixtures. Data from Henshaw et al. [28] also shows that this trend continues for even lower ammonia content flames. When keeping within this optimal equivalence ratio range, NO emissions can be kept below 100 ppm while NH_3 emissions can be maintained at around 50–200 ppm. These are suitable conditions for the first stage of multistage combustion. Previous studies [36,52] have shown that accurate control of NO in the first stage of a two-stage rich-lean configuration is the key to maintaining low NO at downstream emissions at the combustor outlet and the remaining NO can be reduced through deNOx reactions with NH_3 in the second stage. Work by Khateeb et al. [24] also recommends rich first-stage ammonia/methane combustion for improved stability, however other sources [22,23], suggest alternative approaches such as stratified injection configuration and combustor designs minimising
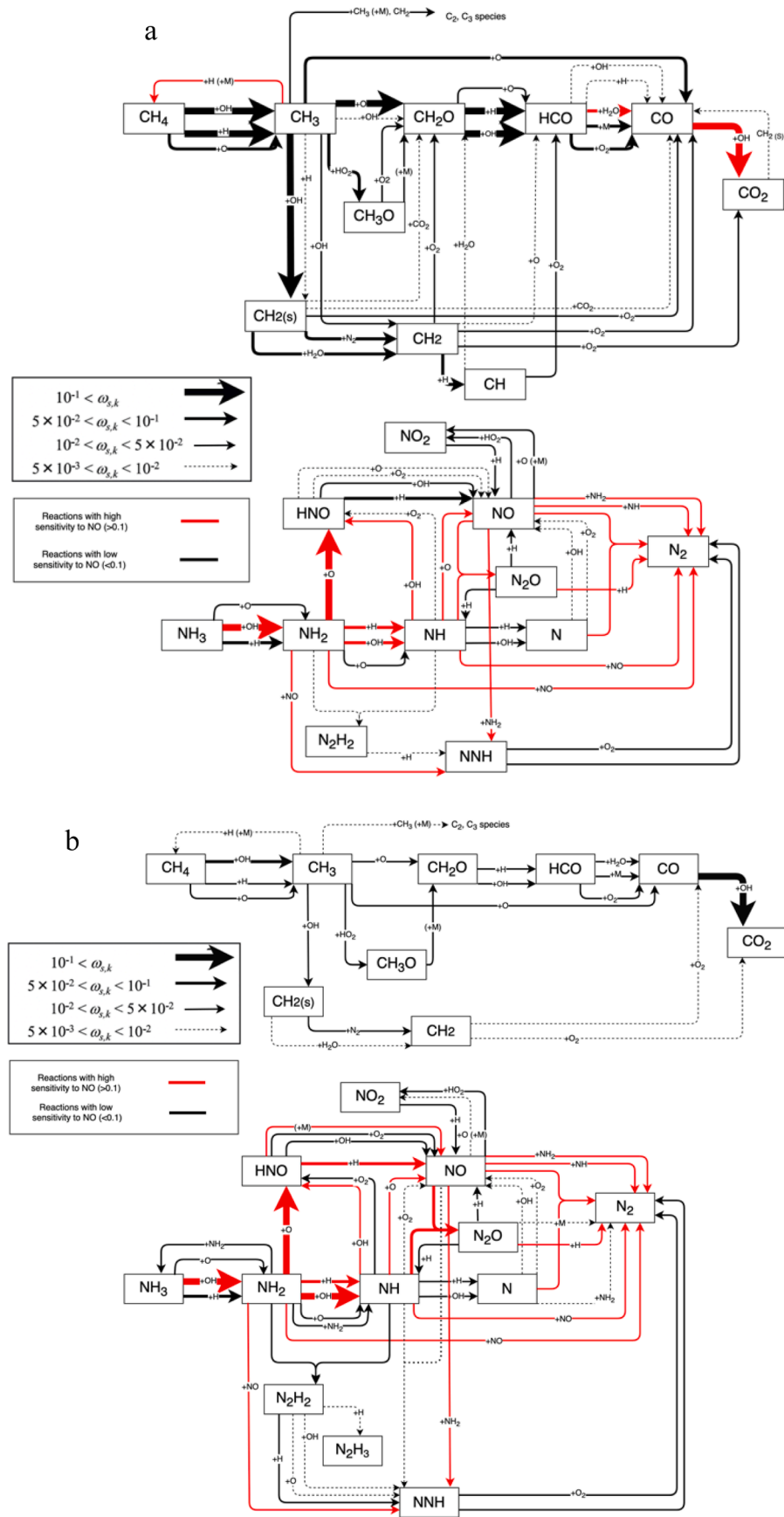
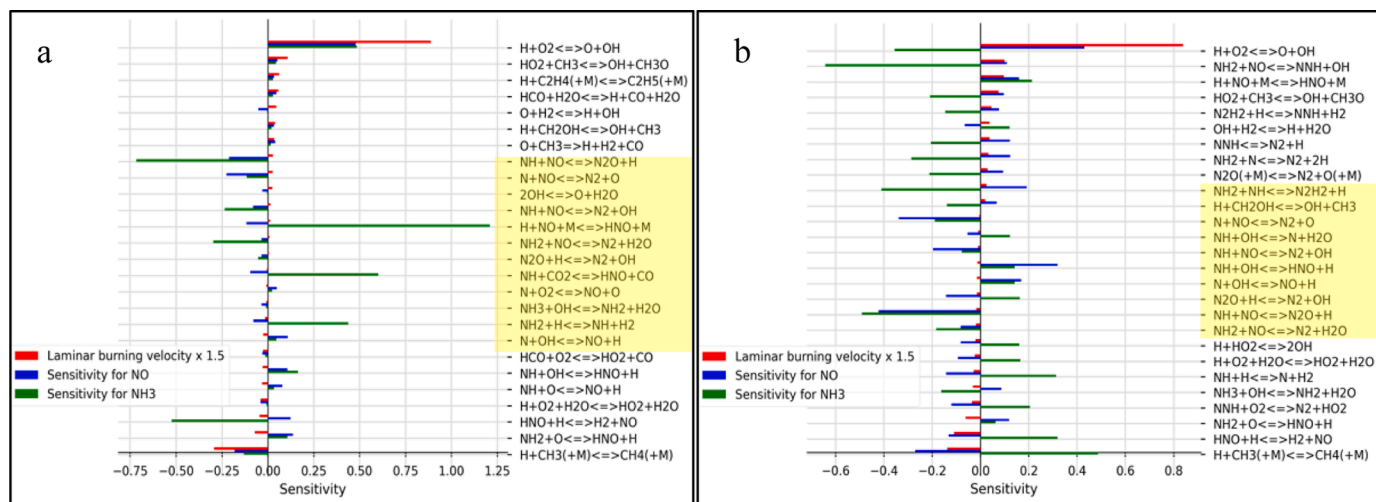**Fig. 10.** Reaction path diagram of NH_3/CH_4 flames at $E_{NH3} = 20\%$ (a) and 60% (b) at $\varphi=0.85$.

Fig. 11. Reactions with highest NO sensitivity and their corresponding NH_3 sensitivity, ordered by laminar velocity for E_{NH3} = 20% (a) and 60% (b) at φ=1.15, using the mechanism of Okafor et al.

wall heat loss are recommended to ensure simultaneously low NOx and NH_3 emissions.

Fig. 5 presents this data in terms of heat ratio. The data shows that at an equivalence ratio of 0.9, peak emissions occur at a 40% heat ratio, with richer flames peaking further towards the 10% heat ratio. These results agree with the work of Ramos et al. [25] which reported increasing near stoichiometry NO emissions at around E_{NH3} = 50%.

Other harmful product gas emissions are reported in Fig. 6. This includes nitrogen oxide (NO_2) which is a toxic gas and a precursor to acid rain, nitrous oxide (N_2O) which is a greenhouse gas with 20-year global warming potential (GWP_{20}) 280 times that of CO_2 [37], carbon monoxide, and hydrogen cyanide (HCN) which is lethal to humans even in small concentrations (with LC50 of 100–300 ppm [38]).

NO_2 emissions followed a similar trend as with NO, with peak emissions occurring at approximately φ=0.8. However, these emissions remained below 200 ppm and so were a less significant contributor to NOx compared to the peak NO emissions of around 8000 ppm. N_2O emissions also remained low within the examined conditions in this study and insignificant contributor to overall NOx. At E_{NH3} = 20%, there may be some indication of N_2O increasing in the very lean region, as previously captured in emissions trends of swirl-stabilised flames [21]. However, as this rise was at the edge of the stability region of the flame, it was not within the scope of this study.

Finally, HCN followed a close trend to NH_3 whereby the low HCN window moved further to the rich region, with the increase also occurring at equivalence ratios of 1.2 to 1.35 for corresponding heat ratios of E_{NH3}=60% to 10%. The trend of decreasing NO with increasing HCN at rich conditions has previously been described by Glarborg et al. [18] as being related to the conversion of HCN to prompt-NO slowing at richer conditions due to decrease in availability of O atom concentration. Furthermore, at these conditions, the reaction of NO with amines or CH_x radicals to produce HCN become more dominant. Although the low NOx and NH_3 window (at equivalence ratios of 1.2 to 1.35) also occurs in the low HCN region, care should be taken to consider the increasing CO emissions at this equivalence ratio range.

Reaction analysis

E_{NH3}=20% and E_{NH3}=60% flames at a rich equivalence ratio of 1.15 and a lean equivalence ratio of 0.85 were considered for further analysis. The equivalence ratio of 1.15 captures trends closer to the optimal operating condition, where NO production has significantly decreased, and allowing for a comparison between lean and rich flame behaviour at these heat ratios. The two ammonia heat fractions are taken at either

side of the ammonia ratio of E_{NH3}=30%−40% (peak NO emissions) to capture changes in chemistry across these different conditions. Fig. 7 shows the performance of the three numerical models against the experimental NO emissions, with the mechanisms of Okafor et al. and UCSD showing a significantly improved performance over the GRI-3.0 mechanism. For E_{NH3}=60%, the mechanism of Okafor et al. over-predicted NO emissions while the UCSD mechanism underpredicted emissions, however both were relatively accurate in describing the overall trend. At rich, high low ammonia fuel content conditions, the mechanisms almost converge to the same values. However, GRI-3.0 mechanism fails to describe the low unburnt ammonia production window for both types of blends, overpredicting NO emissions for low ammonia content, and underpredicting for high ammonia content flames.

Fig. 8 shows the performance of the three numerical models against the experimental NH_3 emissions, with satisfactory performance for Okafor's and UCSD mechanisms. However, GRI3.0 mechanism, over-predicts NH_3 emissions at high ammonia content flames and under-predicts ammonia emissions for low ammonia content blends.

Since Okafor's mechanism satisfactory performance overall and was developed specifically for NH_3/CH_4 blends, Okafor's mechanism was selected for further analysis. As demonstrated by Figs. 7 and 8, Okafor's mechanism adequately predicts NH_3 emissions in the rich region, but needs further improvement for NO. Therefore, NH_3 and NO species were considered in the sensitivity analysis. Okafor's mechanism was developed and optimised based on laminar burning velocity, therefore, the next section aims to identify reactions with low sensitivity to laminar burning velocity and NH_3 but high sensitivity to NO.

Fig. 9 shows the reactions with highest sensitivity to NO, with the yellow regions marking reactions that have high sensitivity to NO and low sensitivity to laminar burning velocity. As previously mentioned, as Okafor's mechanism has good accuracy in modelling laminar burning velocity of NH_3/CH_4 blends, therefore reactions of interest are those with high NO sensitivity but low laminar burning velocity sensitivity. Fig. 9 shows that for lean conditions, many reactions involving NH and NH_2 species with O, H, NO and O_2 had a high sensitivity for NO without having a strong effect on the laminar burning velocity.

Fig. 10 shows the reaction path diagrams for lean conditions, where the thickness of the arrow corresponds to the magnitude of the rate of species production from reaction k integrated over the whole length of the computational domain, $\omega_{s,\ k}$ (mol/(m^2 s)), considering only the reactions that have $\omega_{s,\ k} > 5 \times 10^{-3}$ mol/(m^2s). Reactions with high sensitivity to NO are marked in red.

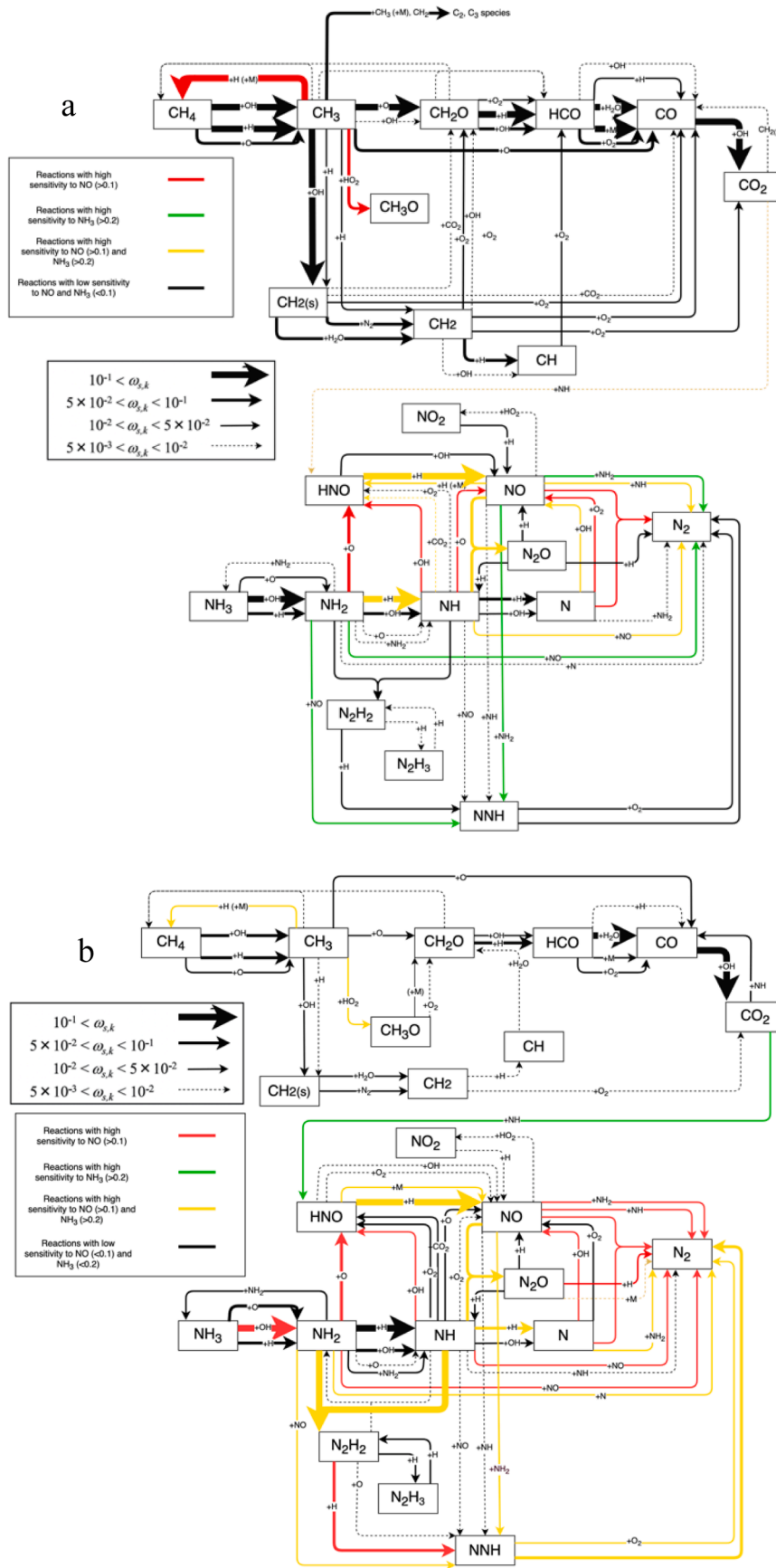Fig. 10 shows that the oxidation pathway of ammonia NH3→NH_x

Fig. 12. Reaction path diagram of NH_3/CH_4 flames at $E_{NH3} = 20\%$ (a) and 60% (b) at $\varphi=1.15$.

Table 1
List of reactions which can be used for the adjustment of the Okafor mechanism.

Reaction	Number	Condition of interest
$N + NO \Leftrightarrow N_2 + O$	(R1)	All conditions
$NH_2 + O \Leftrightarrow HNO + H$	(R2)	Lean, ammonia flame
$NH + OH \Leftrightarrow HNO + H$	(R3)	All but rich methane flames
$NH + NO \Leftrightarrow N_2O + H$	(R4)	All but rich methane flames
$NH_2 + OH \Leftrightarrow NH + H_2O$	(R5)	Lean flames
$NH + NO \Leftrightarrow N_2 + OH$	(R6)	All
$N_2O + H \Leftrightarrow N_2 + OH$	(R7)	All
$NH_2 + NO \Leftrightarrow N_2 + H_2O$	(R8)	Methane flames
$NH_3 + OH \Leftrightarrow NH_2 + H_2O$	(R9)	All
$NH + O \Leftrightarrow NO + H$	(R10)	All
$NH_2 + H \Leftrightarrow NH + H_2$	(R11)	All but rich ammonia
$NH + O_2 \Leftrightarrow HNO + O$	(R12)	Lean ammonia flames
$NH + CO_2 \Leftrightarrow HNO + CO$	(R13)	Rich methane flames
$N + OH \Leftrightarrow NO + H$	(R14)	Rich flames
$HCO + O_2 \Leftrightarrow HO_2 + CO$	(R15)	Methane flames
$H + HO_2 \Leftrightarrow 2OH$	(R16)	Rich ammonia flames
$N + O_2 \rightarrow NO + O$	(R17)	All but rich ammonia

Table 2
List of updated reaction constants for Okafor mechanism. The rate coefficient is given by the modified Arrhenius equation $k = AT^n exp^{\left(\frac{-E_a}{RT}\right)}$, where all units are in cm, mol, s, cal and K.

Reaction	Number	A	n	E_a	Source
$N + NO \rightarrow N_2 + O$	(R1)	9.4×10^{12}	0.140	0	[40]
$NH_2 + O \rightarrow HNO + H$	(R2)	6.6×10^{14}	−0.5	0	[42]
$NH + OH \rightarrow HNO + H$	(R3)	4×10^{13}	0	0	[42]
$NH + NO \rightarrow N_2O + H$	(R4)	1.8×10^{14}	−0.351	−244	[43]
$NH_2 + OH \rightarrow NH + H_2O$	(R5)	3.3×10^6	1.949	−217	[43]
$N_2O + H \Leftrightarrow N_2 + OH$	(R7)	6.4×10^7	1.835	13,492	[43]
$NH_2 + NO \rightarrow N_2 + H_2O$	(R8)	2.6×10^{19}	−2.369	870	[44]
$N + OH \Leftrightarrow NO + H$	(R14)	3.8×10^{13}	0	0	[45]
$N + O_2 \rightarrow NO + O$	(R17)	5.9×10^9	1	6280	[41]

species and their reactions to form NOx have high NO sensitivity and formation at all conditions. The HCO → CO_2 and CH_3 → CH_4 conversion pathways have more influence in the production of NO for low ammonia content flames, with the HNO→ NO conversion pathway being more significant in the production of NO in high ammonia content flames. However, for both fuel blends, the formation of NO occurs primarily with HNO and NH as intermediates in the fuel-N pathway. At these lean conditions, there is little direct interaction between CH_x and NH_x species to form NOx species, and instead, the methane oxidation and ammonia oxidation pathways compete for the availability of radicals. An example of this is the close link between lean N_2O and NO trends through the primary NO_2 production route NO + HO_2 → NO_2 + OH, which shares HO_2 radicals with the CH_3O production route CH_3 + HO_2 → CH_3O + OH, as also noted by other studies [39].

In Fig. 11 and Fig. 12 the analysis was repeated but for rich conditions. At these conditions, HNO and NH intermediates are as significant to the production of NO, however reactions involving NH_2 →NNH and NO→NNH also became more significant as ammonia content increases. On the other hand, for low ammonia content flames, CH_3O has a greater sensitivity to NO. This is the only condition at which the direct interaction of hydrocarbons with NH_x species deemed significant to NO formation through (R13), given as CO_2+NH→HNO+CO. For high ammonia content flames, the N_2H_2 species has a higher production rate and a more significant influence on NO emissions.
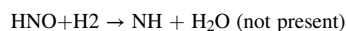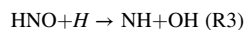
The contributing routes to NO production/consumption across fuel ratios and equivalence ratios can explain the net formation trends given by Zhang et al. [50]. This source has shown that at lean equivalence ratios, HNO (i.e. reactions of HNO with OH and O_2) is the primary

formation, route across all ammonia fuel fractions. However, at an equivalence ratio of 1.2, this source suggests the route of primary production is through NH_i (i.e. reactions of NH and NH_2 with O_2 and O) with no contribution from thermal NO routes at almost any condition. Reaction path analysis in the present study explains that the 2nd and 3rd Zel'dovich production routes are slightly significant in NO production, especially at rich conditions (equivalence ratio of 1.15), but the 1st Zel'dovich reaction for NO consumption N_2+O=NO+N, counters the 2nd and 3rd Zel'dovich reactions N+O_2=NO+O, N+OH = NO +H formation reactions.

Table 1 lists the reactions with low sensitivity to laminar burning velocity and high sensitivity to NO (and NH_3) are detailed in Table 2. These reaction rate constants were reviewed against literature for the improvement of emissions results in Okafor's reaction mechanism.

Constants were updated only for the reactions which improved performance or recent values were available in literature, mostly for thermal NO reactions and routes towards NO production through both HNO and NH as intermediaries. The impact of changing each individual rate constant is provided in the supplementary materials.

However, it was challenging to update constants specific only to rich methane flames. Of particular interest for these conditions was R13, a reaction which is part of the subset of three competing HNO pathways:

HNO+H → NH+OH (R3)

HNO+CO → NH+CO_2 (R13)

HNO+H2 → NH + H_2O (not present)

HNO is mostly formed through reactions of NO and H, H_2 and of the alternative pathways listed above, studies [48, 51] have shown that only R3 is predominant to HNO production. The reaction of HNO with H_2 is not included in the mechanism of Okafor et al. Despite this, R13 is present in the mechanism shown to be significant in rich N_2O production. Removing this reaction from the mechanism reduces N_2O levels in the rich region to below 10 ppm very slightly improves NO prediction in the rich region for low ammonia content flames. Due to the large measurement range of the N_2O on the emissions analyser, N_2O has a large uncertainty compared to measured and modelled values. Therefore, to better assess the prediction capability of the revised mechanism for N2O production, the resolution of N_2O measurements should be improved in future studies.

Fig. 13 describes the performance of the updated mechanism (of 59 species and 354 reactions) for predicting NO and NH_3 emissions, showing improved performance for N_2O and NO, especially for lean flames. Furthermore, awareness of the high NH_3 sensitivity reactions when modifying the rate constants resulted in a relatively small change in NH_3 emissions. Finally, the deviation of the laminar burning velocity values from the original were maintained at less than 1%.

For future development, prediction of NO in the rich region for high methane content flames should be improved to provide an even more accurate model for emissions trends of these blends. One suggestion, given by a study of fuel rich ammonia chemistry [48] suggests that some extended reactions of HCN formation and consumption from CH_xNH_y and CH_xCN species is relevant for these conditions. However, this study also states that only a small portion of the products feed the amine pool and contribute to NO, and hence have very minimal NO sensitivity. An analysis of reaction kinetics at stoichiometry by Brackmann et al. [29] also suggests that while these reactions do not appear to have high sensitivity to NO, they do have some sensitivity to the amine pool. Other amine-hydrocarbon interactions such as CH_3+NH_3→CH_4+NH_2 could also be considered.

Though beyond the scope of this work, for future development of rich methane flames, reactions in the formation of CO and CO_2 species should also be evaluated. Studies note that [48,30] that the addition of CO to the reaction zone acts to increase O/H radical pool, while the addition of CO_2 acts to decrease the radical pool and decrease hence NO
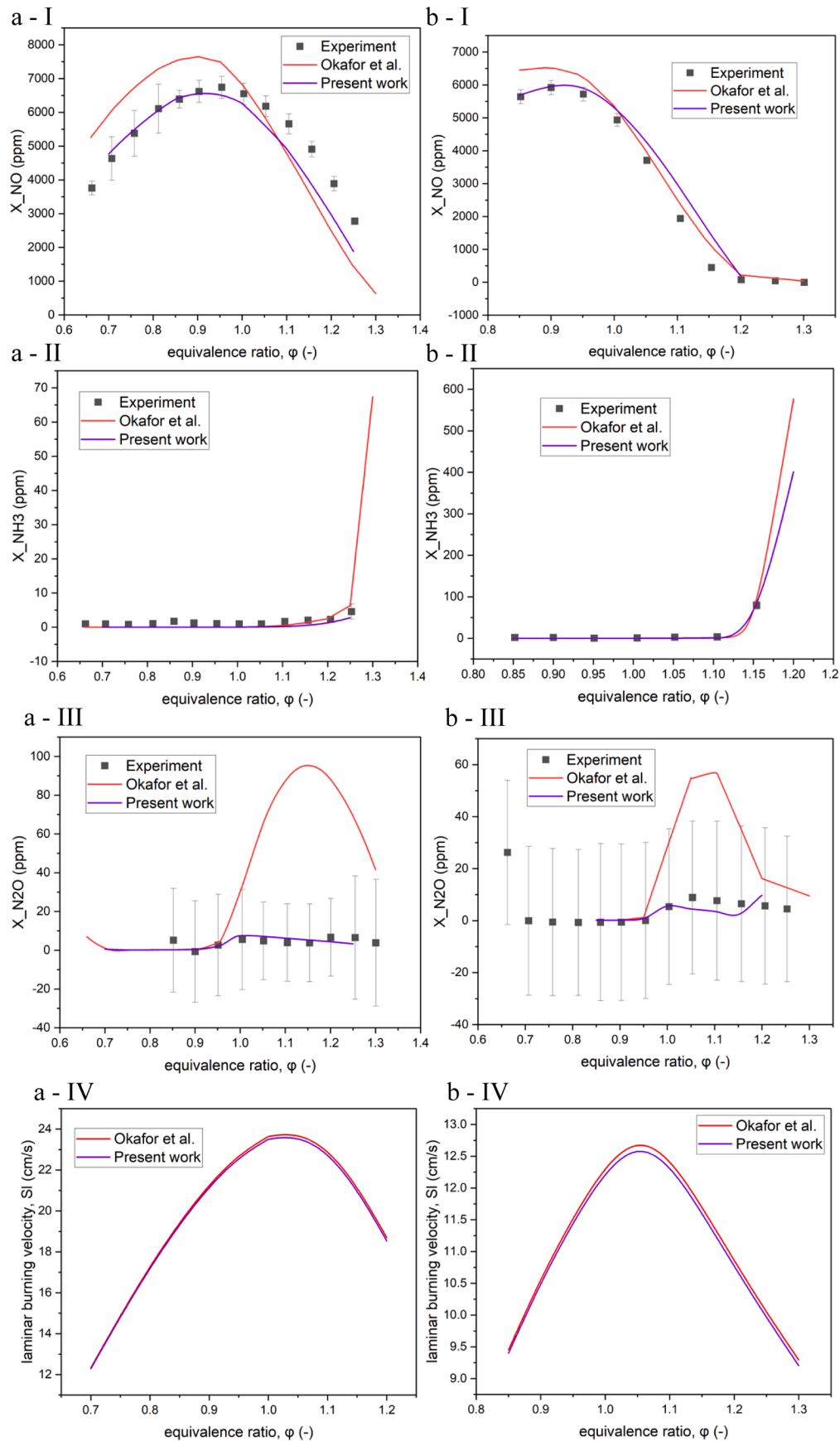
Fig. 13. Updated values of NO, NH$_3$, N$_2$O and laminar burning velocity for NH$_3$/CH$_4$ flames at E$_{NH3}$ = 20% (a) and 60% (b) relative to experimental results.
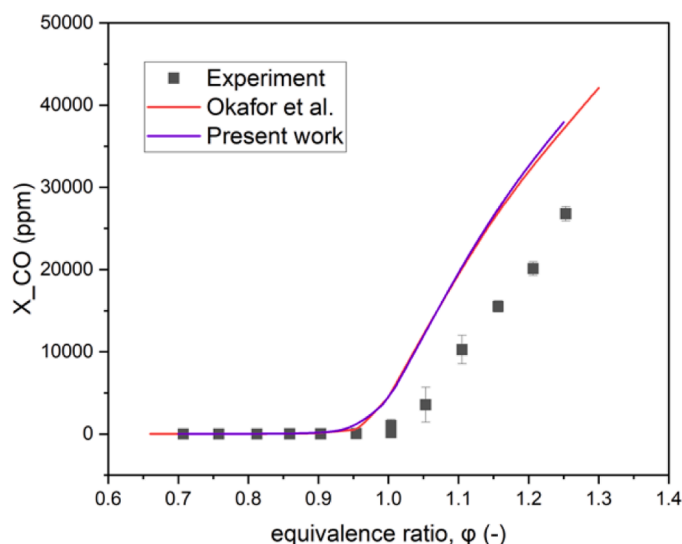
Fig. 14. A comparison of numerical CO results for NH_3/CH_4 flames at $E_{NH3} = 20\%$ relative to experimental results.

emissions. Fig. 14 shows that both the Okafor's original mechanism and the updated version both overpredicted CO emissions by significant values of 2000 ppm and 6000 ppm at $E_{NH3} = 20\%$ at equivalence ratios of 1.10 and 1.25 respectively. As discussed earlier, NO and OH emissions are also highly correlated. Therefore, an increase in concentration of downstream OH of rich methane flames would also increase the consumption of CO and CN and promote higher NO production, closer to the values predicted by the experiment.

However, when adding further reactions and more complex species to the mechanism, the authors acknowledge the compromise in balancing the computational requirements of the mechanism with performance.

Conclusions

In this study, the product gas characteristics of laminar ammonia/methane flames were studied. The following conclusions have been made:

- Product gas trends (measuring NH_3, NO, N_2O, NO_2, CO, CO_2, H_2O, O_2 and HCN) were measured, suitable for mechanism validation through a one-dimensional numerical flame model.
- The optimal equivalence ratio emissions was identified for ammonia heat ratios between 10% to 60% E_{NH3}, in a laminar flame configuration for the first time. It was found that an equivalence ratio range from ~1.35 to 1.20, with increasing ammonia content could maintain NO emissions below 100 ppm and NH_3 emissions at around 50–200 ppm. These are the relevant conditions for powering first stage of a two-stage rich-lean combustor.
- Peak NO emissions occurred at near stoichiometry, with $E_{NH3} = 30\%$, 40% flames having the highest emissions of the blends tested and high ammonia content flames having a narrower peak than the low ammonia content flames.
- Generally, the mechanisms of Okafor et al. and UCSD were found to be good predictors of NH_3 and NO emissions, however all mechanisms significantly underpredicted NO emissions in rich, low ammonia content flames.
- A sensitivity and reaction path analysis highlighted key reactions impacting NO production was conducted for the mechanism of Okafor et al. Improvements to reaction rate constants have been suggested, showing improved performance for N_2O and lean NO trends for all blends.

- However, in the rich region, modelled NO values were less responsive to changes in reaction constants, suggesting the need for further studies focused on the improvement of NO and CO chemistry in rich, low ammonia content flames.

CRediT authorship contribution statement

Marina Kovaleva: Methodology, Formal analysis, Investigation, Writing – original draft. **Akihiro Hayakawa:** Conceptualization, Methodology, Formal analysis, Supervision, Validation, Writing – review & editing. **Sophie Colson:** Writing – review & editing, Investigation. **Ekenechukwu C. Okafor:** Writing – review & editing, Formal analysis. **Taku Kudo:** Resources, Investigation. **Agustin Valera-Medina:** Supervision, Project administration. **Hideaki Kobayashi:** Validation, Project administration.

Declaration of Competing Interest

The authors declare that they have no known competing financial interests or personal relationships that could have appeared to influence the work reported in this paper.

Supplementary materials

Supplementary material associated with this article can be found, in the online version, at doi:10.1016/j.jfueco.2022.100054.

References

[1] Kobayashi H, Hayakawa A, Somarathne KDKA, Okafor EC. Science and technology of ammonia combustion. Proc Combust Inst 2019;37:109–33.
[2] Valera-Medina A, Xiao H, Owen-Jones M, David WIF, Bowen PJ. Ammonia for power. Prog Energy Combust Sci 2018;69:63–102.
[3] Valera-Medina A, Amer-Hatem F, Azad AK, Dedoussi IC, de Joannon M, Fernandes RX, Glarborg P, Hashemi H, He X, Mashruk S, McGowan J, Mounaim-Rouselle C, Ortiz-Prado A, Ortiz-Valera A, Rossetti I, Shu B, Yehia M, Xiao H, Costa M. Review on ammonia as a potential fuel: from synthesis to economics. Energy Fuels 2021.
[4] Crolius S. Ammonia energy mainstreaming expands to governments. Ammon Energy Assoc 2019.
[5] T. and I. Japanese Ministry of Economy. METI unveils green growth strategy to support Japan's 2050 carbon neutral goal. METI Online Site 2021.
[6] Brown T. Japan's road map for fuel ammonia. Ammon Energy Assoc 2021.
[7] UK Department for Transport, Maritime 2050. Navigating the future. GovUk 2019.
[8] Brown T. Green ammonia plants. Commercially Available Today 2018.
[9] T. Brown, Green ammonia plants win financing in Australia and New Zealand (2020).
[10] S. Seznec, Jean-François; mosis, will Saudi Arabia build the world's largest green hydrogen and ammonia plant? (2020).
[11] The Royal Society, Ammonia: zero-carbon fertiliser, fuel and energy store (2020).
[12] Hayakawa A, Goto T, Mimoto R, Kudo T, Kobayashi H. NO Formation/reduction mechanisms of ammonia/air premixed flames at various equivalence ratios and pressures. Mech Eng J AdvPub 2015.
[13] Colson S, Hayakawa A, Kudo T, Kobayashi H. Extinction characteristics of ammonia/air counterflow premixed flames at various pressures. J Therm Sci Technol 2016;11. JTST0048–JTST0048.
[14] Ichimura R, Hadi K, Hashimoto N, Hayakawa A, Kobayashi H, Fujita O. Extinction limits of an ammonia/air flame propagating in a turbulent field. Fuel 2019;246:178–86.
[15] Hayakawa A, Goto T, Mimoto R, Arakawa Y, Kudo T, Kobayashi H. Laminar burning velocity and Markstein length of ammonia/air premixed flames at various pressures. Fuel 2015;159:98–106.
[16] Mendiara T, Glarborg P. Ammonia chemistry in oxy-fuel combustion of methane. Combust Flame 2009;156:1937–49.

[17] Okafor E, Naito Y, Colson S, Ichikawa A, Kudo T, Hayakawa A, Kobayashi H. Experimental and numerical study of the laminar burning velocity of CH$_4$ – NH$_3$ – air premixed flames. Combust Flame 2018;187:185–98.

[18] Glarborg Peter, Miller James A, Ruscic Branko, Klippenstein Stephen J. Modeling nitrogen chemistry in combustion. Prog Energ Combust Sci 2018;67:31–68.

[19] Okafor EC, Naito Y, Colson S, Ichikawa A, Kudo T, Hayakawa A, Kobayashi H. Measurement and modelling of the laminar burning velocity of methane-ammonia-air flames at high pressures using a reduced reaction mechanism. Combust Flame 2019;204:162–75.

[20] Gotama GJ, Hayakawa A, Okafor EC, Kanoshima R, Hayashi M, Kudo T, Kobayashi H. Measurement of the laminar burning velocity and kinetics study of the importance of the hydrogen recovery mechanism of ammonia/hydrogen/air premixed flames. Combust Flame 2022;236:111753.

[21] Okafor EC, Somarathne KDKA, Ratthanan R, Hayakawa A, Kudo T, Kurata O, Iki N, Tsujimura T, Furutani H, Kobayashi H. Control of NOx and other emissions in micro gas turbine combustors fuelled with mixtures of methane and ammonia. Combust Flame 2020;211:406–16.

[22] Valera-Medina A, Marsh R, Runyon J, Pugh D, Beasley P, Hughes T, Bowen P. Ammonia–methane combustion in tangential swirl burners for gas turbine power generation. Appl Energy 2017;185:1362–71.

[23] Somarathne KDKA, Okafor EC, Hayakawa A, Kudo T, Kurata O, Iki N, Kobayashi H. Emission characteristics of turbulent non-premixed ammonia/air and methane/air swirl flames through a rich-lean combustor under various wall thermal boundary conditions at high pressure. Combust Flame 2019;210:247–61.

[24] Khateeb AA, Guiberti TF, Wang G, Boyette WR, Younes M, Jamal A, Roberts WL. Stability limits and NO emissions of premixed swirl ammonia-air flames enriched with hydrogen or methane at elevated pressures. Int J Hydrogen Energy 2021;46:11969–81.

[25] Ramos CFilipe, Rocha RC, Oliveira PMR, Costa M, Bai X-S. Experimental and kinetic modelling investigation on NO, CO and NH3 emissions from NH3/CH4/air premixed flames. Fuel 2019;254:115693.

[26] Rocha RC, Zhong S, Xu L, Bai X-S, Costa M, Cai X, Kim H, Brackmann C, Li Z, Aldén M. Structure and laminar flame speed of an ammonia/methane/air premixed flame under varying pressure and equivalence ratio. Energy Fuels 2021;35:7179–92.

[27] Konnov AA, Dyakov IV, Ruyck JDE. Probe sampling measurements of NO in CH$_4$+O$_2$+N$_2$ flames doped with NH$_3$. Combust Sci Technol 2006;178:1143–64.

[28] Henshaw PF, D'Andrea T, Mann KRC, Ring DS-K. Premixed ammonia-methane-air combustion. Combust Sci Technol 2005;177:2151–70.

[29] Brackmann C, Nilsson EJK, Nauclér JD, Aldén M, Konnov AA. Formation of NO and NH in NH$_3$-doped CH$_4$ + N$_2$ + O$_2$ flame: experiments and modelling. Combust Flame 2018;194:278–84.

[30] Mendiara T, Glarborg P. Ammonia chemistry in oxy-fuel combustion of methane. Combust Flame 2009;156:1937–49.

[31] Hayakawa A, Hirano Y, Okafor EC, Yamashita H, Kudo T, Kobayashi H. Experimental and numerical study of product gas characteristics of ammonia/air premixed laminar flames stabilized in a stagnation flow. Proc Combust Inst 2021;38:2409–17.

[32] Hayakawa A, Hirano Y, Ichikawa A, Matsuo K, Kudo T, Kobayashi H. Novel dilution sampling method for gas analysis with a low sampling rate. Mech Eng J 2020;7:19–193.

[33] ANSYS. ANSYS chemkin-pro R1. 2021.

[34] F.A. William, S. Kalyanasundaram, R.J. Cattolica, Chemical-Kinetic Mechanisms for Combustion Applications, San Diego Mech. Web Page, Mech. Aerosp. Eng. Combustion Res. Univ. Calif. San Diego. (2012).

[35] G.P. Smith, D.M. Golden, M. Frenklach, N.W. Moriarty, B. Eiteneer, M. Goldenberg, C.T. Bowman, R.K. Hanson, S. Song, W.C. Gardiner, Jr., V.V. Lissianski, Z. Qin, http://www.me.berkeley.edu/gri_mech/.

[36] Somarathne KDKA, Okafor EC, Sugawara D, Hayakawa A, Kobayashi H. Effects of OH concentration and temperature on NO emission characteristics of turbulent non-premixed CH4/NH3/air flames in a two-stage gas turbine like combustor at high pressure. Proc Combust Inst 2021;38:5163–70.

[37] 2021 United Nations Framework Convention on Climate Change. Global warming potentials. 2022 (IPCC Second Assessment Report), (n.d.) https://elsevier.proofcentral.com/en-us/landing-page.html?token=8069a0cdf90d8f685b0830d94563b8.

[38] Acute Exposure Guideline Levels for Selected Airborne Chemicals: Volume 2. Washington (DC): National Academies Press (US); 2002. 5, Hydrogen Cyanide: Acute Exposure Guideline Levels. Available from: https://www.ncbi.nlm.nih.gov/books/NBK207601/.

[39] Arunthanayothin S, Stagni A, Song Y, Herbinet O, Faravelli T, Battin-Leclerc F. Ammonia–methane interaction in jet-stirred and flow reactors: an experimental and kinetic modeling study. Proc Combust Inst 2021;38:345–53.

[40] Abian M, Alzueta MU, Glarborg P. Formation of NO from N2/O2 mixtures in a flow reactor: toward an accurate prediction of thermal NO. Int J Chem Kinet 2015;47:518–32.

[41] Fernandez A, Goumri A, Fontijn A. Kinetics of the reactions of N(4S) atoms with O2 and CO2 over wide temperatures ranges. J Phys Chem A 1998;102:168–72.

[42] Miller JA, Smooke MD, Green RM, Kee RJ. Kinetic modeling of the oxidation of ammonia in flames. Combust Sci Technol 1983;34:149–76.

[43] Klippenstein SJ, Harding LB, Glarborg P, Miller JA. The role of NNH in NO formation and control. Combust Flame 2011;158:774–89.

[44] Song S, Hanson RK, Bowman CT, Golden DM. Shock tube determination of the overall rate of NH2 + NO → products in the thermal De-NOx temperature window. Int J Chem Kinet 2001;33:715–21.

[45] Glarborg P, Johnsson JE, Dam-Johansen K. Kinetics of homogeneous nitrous oxide decomposition. Combust Flame 1994;99:523–32.

[46] Chien YC, Escofet-Martin D, Dunn-Rankin D. CO Emission from an impinging non-premixed flame. Combust Flame 2016;174:16–24.

[47] Colson S, Hirano Y, Hayakawa A, Kudo T, Kobayashi H, Galizzi C, Escudié D. Experimental and numerical study of NH3/CH4 counterflow premixed and non-premixed flames for various NH3 mixing ratios. Combust Sci Technol 2021;193:2872–89.

[48] Skreiberg Ø, Kilpinen P, Glarborg P. Ammonia chemistry below 1400 K under fuel-rich conditions in a flow reactor. Combust Flame 2004;136:501–18.

[49] Otomo J, Koshi M, Mitsumori T, Iwasaki H, Yamada K. Chemical kinetic modeling of ammonia oxidation with improved reaction mechanism for ammonia/air and ammonia/hydrogen/air combustion. Int J Hydrogen Energy 2018;43:3004–14.

[50] Zhang M, An Z, Wei X, Wang J, Huang Z, Tan H. Emission analysis of the CH4/NH3/air co-firing fuels in a model combustor. Fuel 2021;291:120135.

[51] Glarborg P, Kristensen PG, Dam-Johansen K, Alzueta MU, Millera A, Bilbao R. Nitric oxide reduction by non-hydrocarbon fuels. Implications for reburning with gasification gases. Energy Fuels 2000;14:828–38.

[52] Okafor EC, Somarathne KDKA, Hayakawa A, Kudo T, Kurata O, Iki N, Kobayashi H. Towards the development of an efficient low-NOx ammonia combustor for a micro gas turbine. Proc Combust Inst 2019;37:4597–606.

[53] Brackmann C, Alekseev VA, Zhou B, Nordström E, Bengtsson P-E, Li Z, Aldén M, Konnov AA. Structure of premixed ammonia + air flames at atmospheric pressure: laser diagnostics and kinetic modeling. Combust Flame 2016;163:370–81.